Dynamics of an axisymmetric liquid bridge close to the minimum-volume stability limit

E. J. Vega,[1] J. M. Montanero,[1] M. A. Herrada,[2] and C. Ferrera[1]

[1]*Department of Mechanical, Energy, and Materials Engineering, University of Extremadura, Avenida de Elvas s/n, E-06071 Badajoz, Spain*

[2]*Department of Aerospace Engineering and Fluid Mechanics, University of Seville, Avenida de los Descubrimientos s/n, E-41092-Sevilla, Spain*

(Received 8 May 2014; published 21 July 2014)

We analyze both theoretically and experimentally the dynamical behavior of an isothermal axisymmetric liquid bridge close to the minimum-volume stability limit. First, the nature of this stability limit is investigated experimentally by determining the liquid bridge response to a mass force pulse for volumes just above that limit. In our experiments, the liquid bridge breakup takes place only when the critical volume is surpassed and is never triggered by the mass force pulse. Second, the growth of the small-amplitude perturbation mode initiating the liquid bridge breakage is measured experimentally and calculated from the linearized Navier-Stokes equations. The results of the linear stability analysis allow one to explain why liquid bridges with volumes just above the stability limit are so robust. Finally, the nonlinear process leading to the liquid bridge breakup is described from both experimental data and the solution of the full Navier-Stokes equations. Special attention is paid to the free-surface pinchoff. The results show that the flow becomes universal (independent of both the initial and boundary conditions) sufficiently close to that singularity and suggest that the transition from the inviscid to the viscous regime is about to take place in the final stage of both the experiments and numerical simulations.

DOI: 10.1103/PhysRevE.90.013015 PACS number(s): 47.55.nk, 47.20.Cq

I. INTRODUCTION

A liquid bridge is a drop of liquid held by surface tension between two solid supports. It can be regarded as the simplest idealization of the configuration appearing in the floating zone technique [1], which endows the study of liquid bridges with great interest not only in fluid mechanics but also in the field of material engineering.

The mechanical behavior of isothermal liquid bridges has frequently been examined over the past few decades both theoretically and experimentally. As far as the static problem is concerned, studies have focused on the calculation of both the liquid bridge equilibrium interface shape [2] and its stability limit [3]. There is a considerable body of literature dealing with the theoretical analysis of linear phenomena in liquid bridges. The eigenfrequencies characterizing the axisymmetric modes of cylindrical and axisymmetric shapes have been calculated semianalytically [4] and numerically [5], respectively, for arbitrary values of the capillary (Ohnesorge) number (see its definition in Sec. II A). More recently, the frequency and damping of lateral oscillations of a viscous axisymmetric liquid bridge have also been determined semianalytically [6]. Experimental studies of the linear behavior of isothermal liquid bridges have been relatively scarce, probably due to the high spatial and temporal resolutions required to examine the experiments under normal gravity conditions [7].

The analysis of nonlinear phenomena in liquid bridges has focused on forced and free oscillations [8], the steady streaming flow due to high-frequency vibration [9], the deformation of stretching bridges [10,11], and the breakup process [12,13], among others. Rivas and Meseguer [14] derived a one-dimensional self-similar solution to study the liquid bridge dynamics close to Plateau-Rayleigh stability. The sensitivity of liquid bridges to axial residual acceleration and mass force pulses have been examined both theoretically [15,16] and experimentally [17,18]. The dynamical stability limits (i.e., those for nonlinear perturbations) can differ significantly from the static ones [15,16,19]. The liquid bridge response to arbitrary axisymmetric and nonaxisymmetric perturbations have recently been investigated by integrating numerically the full Navier-Stokes equations [16,20].

For a given value of the liquid bridge slenderness, there is a volume below which the equilibrium shape becomes unstable. This critical volume hardly depends on the Bond number (see its definition in Sec. II A) for short enough liquid bridges [3]. For slender columns, the equilibrium shape becomes more sensitive to small variations of the Bond number [21] and so does the stability limit [3]. The breakup of inviscid liquid bridges at the minimum-volume stability limit was first analyzed from the slice model [22]. The nonlinear oscillations and the breakup of liquid bridges in this parameter region have recently been examined using both a one-dimensional viscous model [23] and the inviscid Navier-Stokes equations [24]. Neither the linearized nor the full viscous Navier-Stokes equations have been solved to analyze the liquid bridge dynamics at the minimum-volume stability limit.

One of the most suggestive surface-tension-driven flows is that taking place when the interface defining a fluid shape pinches due to a capillary instability. Consider first the pinching of the free surface that separates a liquid shape from a passive ambient. In the final stage of this finite-time singularity, the local fluid typical size goes to zero and the system is expected to lose memory of both initial and boundary conditions and to exhibit a universal behavior characterized by its intrinsic properties [25,26]. Dimensional analysis allows one to infer the scaling power laws characterizing the dynamical regimes arising as the spatial and temporal distances from the singularity vanish [27,28]. These distances must be measured in terms of the viscous length $\ell_\mu = \mu^2/\sigma\rho$ and time $t_\mu \equiv \mu^3/\sigma^2\rho$ [29,30], where μ, σ, and ρ are the liquid viscosity, surface tension, and density, respectively.

For sufficiently small Ohnesorge numbers, the liquid passes through an intermediate stage where both the local spatial and time scales are much smaller than those characterizing the boundary and initial conditions, but much larger than ℓ_μ and

t_μ, respectively. This corresponds to an inviscid regime where capillary pressure and inertia are balanced and the size of the neck region decreases with the time to pinching according to the power exponent 2/3. This universal inviscid behavior has been analyzed theoretically [31–33] and observed experimentally [34,35] over the past few decades. As the system approaches the singularity, the local spatial and time scales eventually become comparable and subsequently smaller than ℓ_μ and t_μ, respectively, and thus extensional viscous stresses come into play [25,26,29,36]. Then the power-law exponent shifts from 2/3 to 1. Finally, thermal noise drives the pinching and alters qualitatively the fluid behavior when the microscopic scale is reached [37,38].

For sufficiently large Ohnesorge numbers, the inviscid intermediate regime is replaced with another scaling solution characterized by a set of irrational exponents [39]. The presence of a viscous outer medium fundamentally changes the final stage of the breakage process. In fact, if one includes viscosity in the external fluid then the asymptotic regime is dominated by surface tension and viscous stresses in the two fluids, while inertia becomes negligible [40]. In this case, the pinchoff is not determined by the local dynamics exclusively, although the nonlocal contribution preserves the self-similarity of the pinching dynamics [41,42]. Doshi *et al.* [43] found that the breakup of a low-viscosity drop in a viscous bath produces an exceptional form of singularity in which a long thread forms prior to pinchoff, which violates universality and retains an imprint of the initial and boundary conditions. This behavior was subsequently found in bubbles quasistatically injected in moderately viscous baths [44,45] and coflowing streams [46]. Finally, the inclusion of non-Newtonian effects [11] gives rise to a variety of phenomena whose characterization allows one to measure both interfacial and rheological properties.

In this paper the dynamics of an isothermal axisymmetric liquid bridge close to its minimum-volume stability limit will be examined both theoretically and experimentally. Several aspects of the problem will be considered: (i) the nature of the minimum-volume stability limit by studying how perturbations affect that limit, (ii) the initial stage of the breakup process by analyzing the growth of the linear perturbation that destabilizes the liquid bridge, and (iii) the final phase of that process, focusing our attention on the local flow at the free-surface pinchoff.

The paper is organized as follows. The theoretical approach and the experimental method used to analyze the problem are described in Secs. II and III, respectively. The results are presented and discussed in Sec. IV. Finally, the paper closes with a summary in Sec. V.

II. THEORETICAL APPROACH

A. Fluid configuration

The fluid configuration considered (Fig. 1) consists of an isothermal mass of liquid of volume $\mathcal{V}$ held between two parallel and coaxial circular supports of radius R placed a distance L apart. Due to the sharpness of their edges, one assumes that the liquid anchors perfectly to those edges, preventing motion of the triple contact line. The liquid bridge is surrounded by air, whose effects can be neglected, and is subjected to the action of gravity, whose magnitude per unit mass is g. The liquid density and viscosity are ρ and μ, respectively, while the surface tension is σ. The initial equilibrium contour of the liquid bridge is characterized by the function $F_0(z)$, which measures the distance between a surface element and the axis of the disks (z axis). The free-surface position during the breakup is characterized by the function $F(z,t)$, which measures that distance at the instant t.

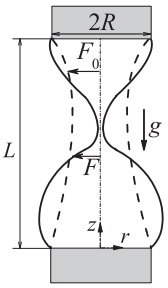

FIG. 1. Liquid bridge configuration.

In this section all the quantities are made dimensionless using the disk radius R, the capillary time $t_0 \equiv (\rho R^3/\sigma)^{1/2}$, and the liquid density ρ as the characteristic length, time, and density, respectively. The dimensionless parameters characterizing the fluid configuration are the slenderness $\Lambda \equiv L/(2R)$, the dimensionless volume $V \equiv \mathcal{V}/(\pi R^2 L)$, the static Bond number $B_0 \equiv \rho g R^2/\sigma$, and the capillary number (defined as the square root of the Ohnesorge number) $C_\mu \equiv \mu(\rho\sigma R)^{-1/2}$. For fixed values of Λ, B_0, and C_μ, there is a minimum value of the liquid bridge volume V below which this fluid configuration becomes unstable [3].

B. Governing equations

We will analyze the liquid bridge dynamics at the minimum-volume stability limit from the axisymmetric, incompressible Navier-Stokes equations

$$(ru)_r + rw_z = 0, \tag{1}$$

$$u_t + uu_r + wu_z = -p_r + C_\mu[u_{rr} + (u/r)_r + u_{zz}], \tag{2}$$

$$w_t + uw_r + ww_z = -p_z + C_\mu[w_{rr} + w_r/r + w_{zz}], \tag{3}$$

where r and z are the radial and axial coordinates, respectively, t is the time variable, u and w are the radial and axial velocity components, respectively, and p is the (hydrostatic) reduced pressure. Subscripts denote hereinafter the partial derivatives. In addition to the regularity conditions ($u = w_r = p_r = 0$ at $r = 0$) and the nonslip boundary conditions at the disks, one considers the kinematic compatibility and equilibrium of tangential and normal stresses at the free-surface position $r = F(z,t)$:

$$F_t + F_z w - u = 0, \tag{4}$$

$$C_\mu \frac{(1 - F_z^2)(w_r + u_z) + 2F_z(u_r - w_z)}{(1 + F_z^2)^{1/2}} = 0, \tag{5}$$

$$p - B_0\, z + \frac{FF_{zz} - 1 - F_z^2}{F(1 + F_z^2)^{3/2}} - \frac{2C_\mu[u_r - F_z(w_r + u_z) + F_z^2 w_z]}{1 + F_z^2} = 0. \tag{6}$$

The boundary condition (6) must be complemented with the anchoring conditions

$$F = 1 \quad \text{at } z = 0,2\Lambda. \tag{7}$$

Finally, the volume of the fluid configuration is prescribed (and conserved), namely,

$$\pi \int_0^{2\Lambda} F^2 dz = 2\Lambda V. \tag{8}$$

Consider an infinitesimal perturbation of the form $\varepsilon f e^{\Omega t}$ ($\varepsilon \ll 1$). Here f stands for the spatial dependence of the perturbation of the free-surface position and velocity and pressure fields, while $\Omega = \gamma + i\omega$ is the corresponding eigenfrequency. If one introduces these perturbations into the above governing equations and neglects terms in ε^2, one gets a set of linear equations for the perturbed fields f, which are written in terms of the liquid bridge equilibrium shape $F_0(z)$. The solution of this eigenvalue problem is a discrete set of oscillations modes that can be calculated numerically.

C. Numerical methods

The nonlinear problem was numerically solved with a spectral method developed in the present work. Use was made of the intrinsic coordinate system (q,s) defined by the coordinate transformation $r = f(s,t)\,q$ and $z = g(s,t)$, where $f(s,t)$ and $g(s,t)$ are the functions that define the parametric curve $r^* = f(s,t)$ and $z^* = g(s,t)$ corresponding to the liquid bridge free-surface position at the instant t. The coordinate s is the free-surface arc length normalized in such a way that $s = 0$ and $s = 1$ correspond to the lower and upper ends of that surface, respectively. By using this coordinate transformation, the fluid domain was mapped onto the computational square domain ($0 \leqslant q \leqslant 1, 0 \leqslant s \leqslant 1$). This square was discretized using n_q Chebyshev collocation points [47] along the q axis and n_s points uniformly distributed along the s axis. We used fourth-order central finite differences to get the derivatives with respect to this last coordinate, except close to the s boundaries, where second-order upwind finite differences were applied. By using this spatial discretization, remarkable accuracy could be obtained with a relatively reduced number of mesh points. The results presented in this paper were obtained with $n_q = 11$ and $n_s = 181$. The (implicit) time advancement was performed using second-order backward differences, with a time step adapted in the course of the simulation. At each time step, the resulting set of $3n_q \times n_s + 2n_s$ discrete nonlinear equations were solved iteratively using the Newton-Raphson method implemented in the MATLAB subroutine FSOLVE. The initial guess for the iterations at each time step was the solution at the previous instant. To trigger the liquid bridge breakup process right at the stability limit, a stable shape with a volume just above the critical one was slightly perturbed by applying a very small mass force. This perturbation was not expected to affect the liquid bridge dynamics close to the free-surface pinchoff.

The linearized problem was solved with the spectral method developed in Ref. [48]. The fluid domain was mapped onto the computational square domain ($0 \leqslant \xi \leqslant 1, 0 \leqslant \eta \leqslant 1$) through the coordinate transformations $[\xi = r/F_0(z), \eta = z/2\Lambda]$. The resulting square was discretized using n_ξ and n_η Chebyshev collocation points [47] along the ξ and η directions, respectively. This spatial discretization yielded high accuracy with a relatively small number of mesh points [48]. The results presented in this paper were obtained with $n_\xi = 10$ and $n_\eta = 70$. This last parameter was increased up to $n_\eta = 190$ to properly resolve the eigenvalue bifurcation close to the minimum-volume stability limit (as will be explained in Sec. IV B). Use was made of the MATLAB subroutine EIGS to calculate the eigenvalues of the system of $3n_\eta \times n_\xi + n_\xi$ discrete linear equations.

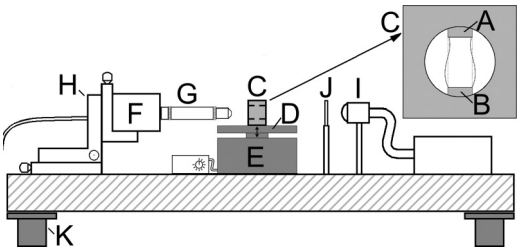

FIG. 2. Experimental apparatus: A, upper needle; B, bottom disk; C, liquid bridge cell; D, vibrating platform; E, electrodynamic shaker; F, camera; G, optical lenses; H, micrometer screws; I, optical fiber; J, frosted diffuser; and K, optical table.

III. EXPERIMENTAL METHOD

Figure 2 shows the experimental setup used in the present study. A liquid bridge of 5-cSt silicone oil (where 1 cSt $\equiv 10^{-2}$ cm^2/s, with $\rho = 917$ kg/m^3, $\sigma = 0.019$ N/m, and $\mu = 0.0046$ kg/ms) was formed between an upper needle (A) and a coaxial bottom disk (B), both about 1 mm in radius and placed in a cubic cell (C). The upper needle was capable of displacement along its axis and was used to feed and remove liquid by using a syringe pump connected to a stepping motor. The cell was mounted on a vibrating platform (D). An electrodynamic shaker (E) produced the vertical motion of the platform when needed. This motion was controlled with a 10-MHz function and arbitrary waveform generator (Agilent, LXI) connected to the power amplifier of the electrodynamic shaker.

Digital images of the liquid bridge were acquired at up to 210 000 frames per second with an exposure time of about 2 μs using a ultra-high-speed complementary metal-oxide semiconductor camera (Photron, FASTCAM SA5) (F). The camera was equipped with a set of optical lenses (G) that consisted of a 10× magnification zoom objective (Mitutoyo) and a system of lenses (Optem Zoom 70 XL) with variable magnification from 0.75× to 5.25×. The magnification obtained ranged approximately from 5.0 to 1.0 μm/pixel. The camera could be displaced both horizontally and vertically using a triaxial translation stage (H) to focus the liquid bridge. The fluid configuration was illuminated from the back side by cool white light provided by an optical fiber (I) connected to a light source. A frosted diffuser (J) was positioned between the optical fiber and the cell to provide a uniformly lit background. All these elements were mounted on an optical table with a pneumatic antivibration isolation system (K) to damp the vibrations coming from the building. The experiments were performed at room temperature and the viscosity value was obtained from the literature for that temperature. The

images of the liquid bridge at equilibrium were processed by the theoretical image fitting analysis axisymmetric interface method [49] to measure the surface tension. The free-surface position was determined by processing the images with a superresolution technique at the subpixel level [50]. In the experiments, the liquid bridge volume was reduced in steps of 0.1 μl by suctioning the liquid at a flow rate of 36 μl/h.

IV. RESULTS

A. Liquid bridge sensitivity to a mass force pulse

The first step of our analysis is to investigate the nature of the minimum-volume stability limit by determining the liquid bridge response to perturbations close to that limit. Specifically, we here analyze experimentally the liquid bridge sensitivity to g-jitter for volumes very close to the critical ones. For this purpose, the following experimental sequence was conducted. A liquid bridge with a given slenderness Λ and initial volume V was formed. Then V was reduced while keeping Λ constant. Each of the resulting equilibrium shapes was perturbed by introducing the mass force pulse described below. The liquid bridge response to that perturbation was analyzed. This sequence was continued until the liquid bridge broke up.

The mass force pulse was applied by moving vertically the liquid bridge cell with an electrodynamic shaker excited with a electric wave generator (see Sec. III). The resulting liquid bridge vertical displacement $Z(t)$ was approximately given by the Boltzmann function

$$\frac{Z}{Z_{\max}} = \frac{e^{t/\Delta t}}{1+e^{t/\Delta t}}. \tag{9}$$

Here the time origin is that at which the liquid bridge is located at the midpoint $Z = Z_{\max}/2$, while $Z_{\max}$ and Δt characterize the pulse magnitude and duration, respectively. The values of these parameters were selected by appropriately choosing the electric wave amplitude.

The liquid bridge displacement $Z(t)$ was precisely measure by processing the images acquired in the course of the experiments. Figure 3(a) shows $Z/Z_{\max}$ as a function of $t/\Delta t$ for five experiments. The mean values of the fitting parameters were $Z_{\max} = 202 \pm 5\ \mu$m and $\Delta t = 3.42 \pm 0.07$ ms [51]. The small measurement uncertainty reflects the high degree of

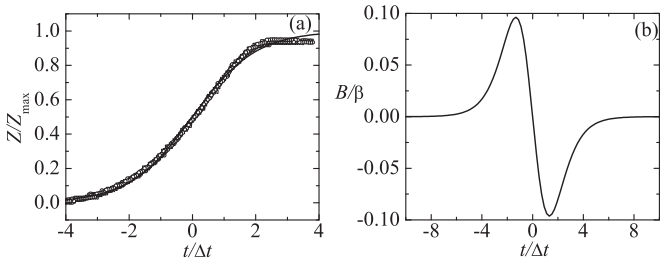

FIG. 3. (a) Liquid bridge displacement $Z/Z_{\max}$ as a function of the (normalized) time $t/\Delta t$ for five experiments. The time origin is that at which $Z = Z_{\max}/2$. Here, $Z_{\max}$ and Δt are the maximum displacement and pulse duration, respectively, and are calculated from the fit (9) in each case. (b) Time dependence of the dynamic Bond number produced by the pulse.

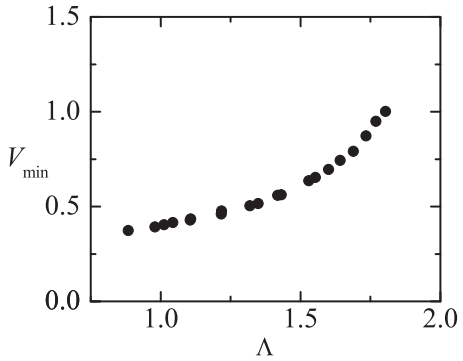

FIG. 4. Minimum volume stability limit $V_{\min}$ as a function of the slenderness Λ for $B_0 = 0.478$ and $C_\mu = 0.0349$.

reproducibility of the displacement produced by the shaker. The pulse duration was on the order of the capillary time t_0. The liquid bridge acceleration gave rise to an inertial force characterized by the dynamic Bond number

$$B = -\tfrac{1}{4}\beta \cosh^{-2}(t/2\Delta t)\tanh(t/2\Delta t), \tag{10}$$

where $\beta = \rho(Z_{\max}/\Delta t^2)\ R^2/\sigma$. Here $B > 0$ ($B < 0$) implies that the inertial force direction is the same as (opposite to) that of gravity. Figure 3(b) shows the time dependence of the dynamic Bond number. In our experiments, the maximum magnitude of this parameter was about 0.081, around 17% of the static value B_0.

Interestingly, all the liquid bridges analyzed in the experimental sequences withstood the perturbation without breaking, i.e., they oscillated and returned to their equilibrium shapes. This occurred even for the shapes obtained right before the minimum-volume stability limit was crossed. In other words, the liquid bridge breakage always took place when the critical volume was surpassed and never when the mass force pulse was applied. Figure 4 shows the minimum volumes reached in the experimental sequences for fixed values of the slenderness Λ. These values agree with those reported in Ref. [3] and the ones calculated here from the linear stability analysis (see Sec. IV B).

B. Linear stability analysis

We devote this section to study the initial phase of the breakage process that occurs when the liquid bridge volume equals the critical one. The free-surface motion at this stage is determined by the growth of the first axial oscillation mode, which becomes unstable for volumes below that threshold. Both the frequency ω and damping rate γ of the first axial oscillation mode were calculated as a function of the liquid bridge volume for fixed values of the rest of parameters. For this purpose, the linearized Navier-Stokes equations were solved with the numerical method described in Sec. II C.

Figure 5 shows the theoretical predictions for ω and γ, as well as the experimental data reported in Ref. [16]. There is good agreement between the two results for all the cases considered. The small discrepancies can be attributed mainly to slight variations of the surface tension characterizing the liquid bridges formed in the experiments. The oscillation frequency ω vanishes for a liquid bridge volume slightly larger than

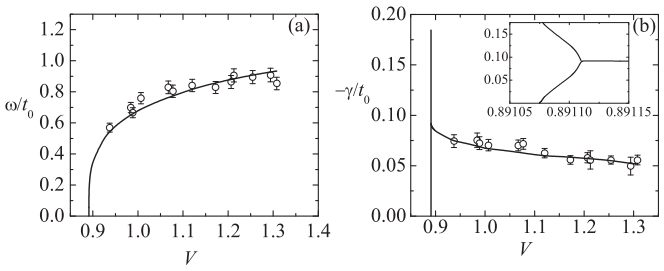

FIG. 5. (a) Frequency ω and (b) damping rate γ characterizing the first axial oscillation mode for $\Lambda = 1.74$, $B_0 = 0.478$, and $C_\mu = 0.0349$. The symbols and solid lines correspond to the experimental and linear stability analysis results, respectively.

the critical one. For that volume, the damping factor curve bifurcates into two practically vertical branches. Then the sign of the dominant branch changes and thus the liquid bridge destabilizes. Interestingly, the range of volumes for which there is overdamping ($\omega = 0$ and $\gamma > 0$) is negligible (on the order of 10^{-5}), and not accesible experimentally. This means that the minimum-volume instability essentially lies in the transition from damped oscillations to an exponential growth. This behavior differs from what happens in, for instance, the Plateau-Rayleigh stability limit, where overdamping can be found in a significant region of the parameter space [4].

We determined experimentally the spatial dependence of the unstable mode by measuring the free-surface evolution right after the instability appears. Figure 6 shows the free-surface deformation $F - F_0$ with respect to the initial shape F_0 at four instants. The results were normalized to prove that the free-surface evolution corresponds to the temporal growth of an unstable mode. The solid line is the numerical result obtained from the linear stability analysis. Owing to the growth of this mode, the upper part of the liquid bridge shrinks while the lower one bulges. For this reason, the upper drop resulting from the liquid bridge breakup is smaller than the lower one.

The linear stability analysis results explain the liquid bridge robustness close to the minimum-volume stability limit

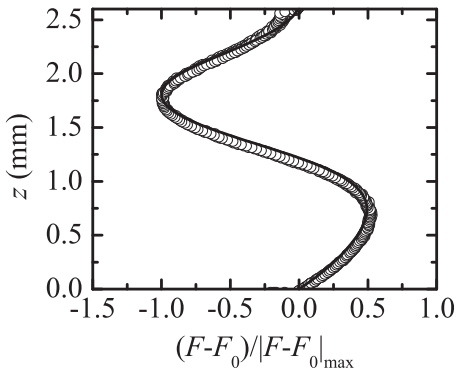

FIG. 6. Initial stage of the liquid bridge deformation for Λ=1.31, $V = 0.500$, $B_0 = 0.478$, and $C_\mu = 0.0349$. The symbols correspond to the normalized free-surface deformation measured at four instants separated by 10 ms. The corresponding values of the maximum deformation were $|F - F_0|_{max} = 26.4$, 28.7, 33.7, and 39.9 μm. The solid line is the numerical result obtained from the linear stability analysis.

(see Sec. IV A). Mass force pulses essentially excite the first axial oscillation mode of the liquid bridge [52]. Close to the minimum-volume stability limit, the oscillation frequency ω of that mode vanishes (Fig. 5) and thus the hydrodynamic time characterizing the liquid bridge evolution becomes much longer than the capillary time t_0. If the pulse duration is of the order of the capillary time (as occurs in our experiments), then it becomes much shorter than the hydrodynamic time. This means that potential energy is suddenly introduced into and removed from the liquid bridge and thus the fluid system does not experience that perturbation. Therefore, g-jitter consisting of isolated pulses with durations smaller than or of the order of the capillary time are not expected to alter the liquid bridge stability. In addition, the fact that the damping rate reaches its maximum value and plunges at the minimum-volume stability limit implies that the liquid bridge becomes more dissipative for volumes just above the critical one.

C. Breakup

In this section we examine the nonlinear breakup process taking place when the liquid bridge volume equals the critical one. Once the initial deformation (described in the previous section) has occurred, a fluid ligament forms in the liquid bridge central part (Fig. 7). This ligament connects the two major drops formed after the breakup. The influence of the gravitational force on the liquid bridge initial shape increases with the slenderness Λ and so does the asymmetry of that initial shape. There is a noticeable imprint of that asymmetry on the ligament shape, which becomes more asymmetric as the liquid bridge slenderness increases.

The liquid bridge free surface pinches at two points. The first pinching takes place at the lower end of the liquid ligament. Subsequently, the free surface pinches at the upper part and thus a satellite droplet forms between the two major drops. This droplet moves upward while oscillating until it touches the upper major drop and coalesces with it. The satellite droplet exhibits slight asymmetry, which is the imprint of the lack of symmetry of the liquid bridge initial shape (and therefore the fluid ligament) due to the gravitational force. The speed at which the droplet displaces

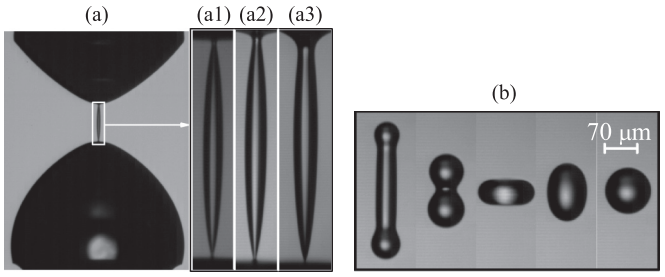

FIG. 7. (a) Ligament formed between the two major drops produced by the breakage of a liquid bridge with $B_0 = 0.478$ and $C_\mu = 0.0349$. The slenderness and volume values are (a1) $\Lambda = 1.07$ and $V = 0.415$, (a2) $\Lambda = 1.36$ and $V = 0.526$, and (a3) $\Lambda = 1.67$ and $V = 0.779$. (b) Sequence of images of the satellite droplet formed after the liquid bridge breakup for $\Lambda = 1.36$ and $V = 0.526$. The images were acquired at $t = 80$, 147, 213, 280, and 347 μs after the first pinching [53].

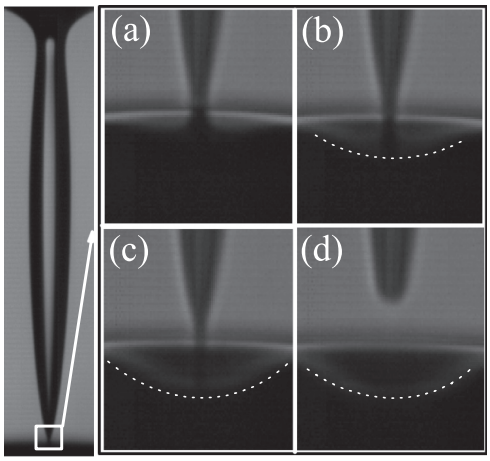

FIG. 8. Final stage of the liquid bridge breakup for $\Lambda = 1.34$, $V = 0.509$, $B_0 = 0.478$, and $C_\mu = 0.0349$. The images correspond to the time to the pinching (a) $\tau = 11.9$, (b) $\tau = 7.14$, (c) $\tau = 2.38$, and (d) $\tau = -2.38$ μs.

and its asymmetry decrease as the liquid bridge slenderness (initial shape asymmetry) decreases. In our experiments, quasisymmetrical droplets practically levitated while viscous stresses damped the free-surface oscillations (Fig. 7). As can be observed, the breakage of a short liquid bridge due to the minimum-volume stability limit may constitute a convenient way of analyzing the evolution of levitating micrometer drops under the action of both capillary and viscous forces.

The final stage of the pinching process is illustrated through the images displayed in Fig. 8, which were acquired at 210 000 frames per second. As can be observed, the free surface delimiting the lower drop retracts and produces a depression right before the pinchoff (the so-called overturning limit [36]). This effect significantly hinders the measurement of the minimum free-surface radius with backlight optical imaging, the method mostly used in this type of experiment [35,44–46].

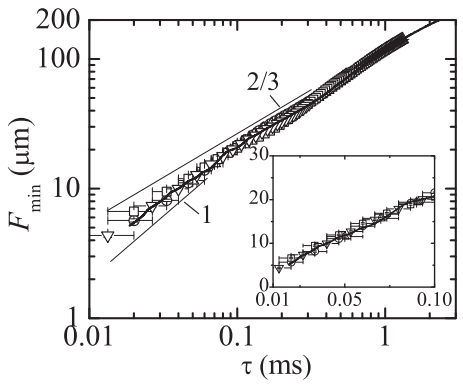

FIG. 9. Minimum value of the free-surface radius $F_{\min}$ as a function of the time to the pinching τ for $B_0 = 0.478$ and $C_\mu = 0.0349$. The circles correspond to $\Lambda = 1.72$ and $V = 0.857$, the up-pointing triangles to $\Lambda = 1.67$ and $V = 0.779$, the squares to $\Lambda = 1.07$ and $V = 0.415$, and the down-pointing triangles to $\Lambda = 1.36$ and $V = 0.526$. The thick solid line is the simulation result for $\Lambda = 1.72$ and $V = 0.857$. The thin solid lines indicate the slopes 1 and 2/3.

Figure 9 shows the minimum value $F_{\min}$ of the free-surface radius as a function of the time to the pinching τ measured for several values of liquid bridge slenderness and volume. As can be observed, the free-surface radius was measured with a small spatial uncertainty for values down to 4 μm (about 2 times the pixel size), which shows the capabilities of the image processing technique [50]. The figure also shows the numerical solution of the full Navier-Stokes equations. As mentioned in Sec. II C, this solution corresponds to the evolution of a quasiunstable liquid bridge whose breakage was induced by a mass force pulse of small magnitude.

Consider the breakup interval for which $F_{\min} \lesssim 100$ μm. Within this interval, the free surface in the pinching region seems to behave independently of the liquid bridge initial shape. Both the theoretical and experimental results indicate that $F_{\min} \sim \tau^{2/3}$ over a great part of the time interval analyzed. This behavior corresponds to the so-called inviscid regime, where the flow is locally dominated by inertia and surface tension [31–35]. For $F_{\min} \lesssim 10$ μm, the curve slope slightly increases, a sign of incipient viscous regime [25,26,29]. In fact, $F_{\min}(\tau)$ exhibits a small curvature when represented on a linear scale (see the inset of Fig. 9). It must be noted that the viscous length and time are $l_\mu \simeq 1.21$ μm and $t_\mu \simeq 294$ ns, respectively, and thus the asymptotic behavior was not expected to appear at that stage. The free surface adopts a double-cone shape next to the pinching region [36,54]. The angle characterizing the upper cone in the last image of the experimental sequences was $\theta = 10 \pm 1^\circ$, while the corresponding simulation prediction was $\theta = 10.4^\circ$. This value is significantly smaller than the asymptotic value $\theta = 18.1^\circ$ in the inviscid case [36,54].

If one keeps only the lowest radial dependence in Eqs. (1)–(6), then the following expression is obtained [29]:

$$\underbrace{\hat{w}_t + \hat{w}\hat{w}_z}_{\text{I}} = \underbrace{-\mathcal{C}_z}_{\text{II}} + \underbrace{3C_\mu(F^2\hat{w}_z)_z F^{-2}}_{\text{III}} - B_0 z, \qquad (11)$$

where $\hat{w}$ is the axial velocity component evaluated at the liquid bridge axis and $\mathcal{C}$ is the local mean curvature of the free surface. The terms I, II, and III correspond to the liquid inertia, capillary force, and viscous force, respectively. Figure 10 shows the "skyline" formed by the magnitudes of these three terms calculated from the simulation in the region next to the first free-surface pinching. The forces were calculated for $\tau = 32$ μs,

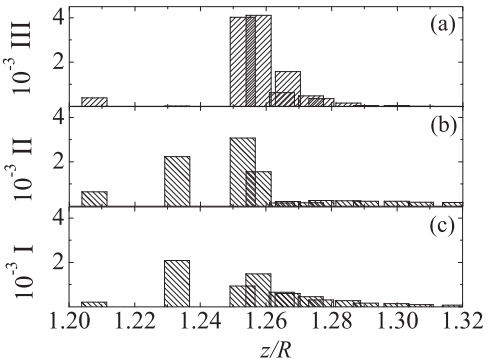

FIG. 10. Magnitude of the three terms indicated in Eq. (11) for $\Lambda = 1.72$, $V = 0.857$, $B_0 = 0.478$, and $C_\mu = 0.0349$. All the quantities were made dimensionless using R, t_0, and ρ.

when the minimum free-surface radius was about 8.3 μm. As can be observed, the viscosity force becomes comparable to and even larger than both the inertia and surface tension next to the pinching point, which confirms that the viscous regime is rising. The gravitational force takes values on the order of 10^{-1} and therefore it can be neglected in the pinching region.

V. CONCLUSION

In this work we studied the dynamical behavior of an isothermal axisymmetric liquid bridge whose volume is just above or below the minimum value leading to its breakup. To this end, we combined the solutions of both the linearized and full Navier-Stokes equations with experimental data obtained with a superresolution image processing technique [50]. The critical role played by the liquid bridge volume in this stability limit was verified experimentally. In fact, equilibrium shapes with volumes just above the threshold withstood the action of g-jitter in all the cases considered. In contrast, all the liquid bridges broke up spontaneously for volumes just below the critical ones.

We calculated both the frequency and damping factor characterizing the first oscillation mode as a function of the liquid bridge volume. The oscillation frequency vanishes before the minimum-volume stability limit is reached. At that point, the damping factor curve bifurcates into the dominant and subdominant branches. For volume slightly smaller than that of the bifurcation point, the dominant branch becomes positive and thus the liquid bridge destabilizes. The interval of the liquid bridge volume within which the oscillations are overdamped is negligible. The comparison between the numerical and experimental results for the unstable mode shows remarkable agreement.

Finally, we analyzed the liquid bridge breakup by solving the full Navier-Stokes equations and by measuring the temporal evolution of the free-surface location. The use of a computationally efficient spectral method on the theoretical side and our superresolution image processing technique on the experimental one allowed us to reach very high spatial and temporal resolutions. Our results confirm the conclusions obtained for other fluid systems [26]. We showed that the local flow taking place at times and distances sufficiently close to the free-surface pinchoff becomes universal, i.e., it is not affected by the initial or boundary conditions. The system undergoes an inviscid collapse over a significant time interval characterized by the power-law exponent 2/3. This regime leads to an asymptotic behavior where the viscosity force becomes comparable to both the inertia and surface tension. Our results barely suggest the birth of this asymptotic regime.

ACKNOWLEDGMENTS

Partial support from the Ministry of Science and Education, Junta de Extremadura, and Junta de Andalucía (Spain) through Grants No. DPI2010-21103, No. GR10047, and No. P08-TEP-04128, respectively, is gratefully acknowledged.

[1] H. C. Kuhlmann, *Thermocapillary Convection in Models of Crystal Growth* (Springer, Berlin, 1999).
[2] J. M. Montanero, G. Cabezas, J. Acero, and J. M. Perales, Phys. Fluids **14**, 682 (2002).
[3] L. A. Slobozhanin and J. M. Perales, Phys. Fluids **5**, 1305 (1993).
[4] J. A. Nicolás and J. M. Vega, Z. Angew. Math. Phys. **51**, 701 (2000).
[5] J. Tsamopoulos, T. Y. Chen, and A. Borkar, J. Fluid Mech. **235**, 579 (1992).
[6] R. Kidambi, Phys. Fluids **24**, 042103 (2012).
[7] E. J. Vega and J. M. Montanero, Phys. Fluids **21**, 092101 (2009).
[8] T. Y. Chen and J. Tsamopoulos, J. Fluid Mech. **255**, 373 (1993).
[9] J. A. Nicolás, D. Rivas, and J. M. Vega, J. Fluid Mech. **354**, 147 (1998).
[10] X. Zhang, R. S. Padgett, and O. A. Basaran, J. Fluid Mech. **329**, 207 (1996).
[11] O. E. Yildirim and O. A. Basaran, Chem. Eng. Sci. **56**, 211 (2001).
[12] J. Meseguer, J. Fluid Mech. **130**, 123 (1983).
[13] J. F. Padday, G. Pétré, C. G. Rusu, J. Gamero, and G. Wozniak, J. Fluid Mech. **352**, 177 (1997).
[14] D. Rivas and J. Meseguer, J. Fluid Mech. **138**, 417 (1984).
[15] Y. Zhang and J. I. D. Alexander, Phys. Fluids A **2**, 1966 (1990).
[16] C. Ferrera, M. A. Herrada, J. M. Montanero, M. Torregrosa, and V. Shevtsova, Phys. Fluids **26**, 012108 (2014).
[17] A. Ramos, F. J. García, and J. M. Valverde, Eur. J. Mech. B: Fluids **18**, 649 (1999).
[18] M. P. Mahajan, M. Tsige, S. Zhang, J. I. D. Alexander, P. L. Taylor, and C. Rosenblatt, Phys. Rev. Lett. **84**, 338 (2000).
[19] J. Meseguer, M. A. González, and J. I. D. Alexander, Microgravity Sci. Tech. **7**, 246 (1994).
[20] L. Ru-Quan and K. Masahiro, Chin. Phys. Lett. **31**, 044701 (2014).
[21] C. Ferrera, J. M. Montanero, and M. G. Cabezas, Meas. Sci. Technol. **18**, 3713 (2007).
[22] J. Meseguer and A. Sanz, J. Fluid Mech. **153**, 83 (1985).
[23] J. M. Perales and J. M. Vega, Phys. Fluids **22**, 112114 (2010).
[24] J. M. Perales and J. M. Vega, Phys. Fluids **23**, 012107 (2011).
[25] J. Eggers, Rev. Mod. Phys. **69**, 865 (1997).
[26] J. Eggers and E. Villermaux, Rep. Prog. Phys. **71**, 036601 (2008).
[27] D. B. Bogy, Annu. Rev. Fluid Mech. **11**, 207 (1979).
[28] J. B. Keller and M. T. Miksis, SIAM J. Appl. Math. **43**, 268 (1983).
[29] J. Eggers, Phys. Rev. Lett. **71**, 3458 (1993).
[30] J. Eggers and T. F. Dupont, J. Fluid Mech. **262**, 205 (1994).
[31] Y.-J. Chen and P. H. Steen, J. Fluid Mech. **341**, 245 (1997).
[32] R. F. Day, E. J. Hinch, and J. R. Lister, Phys. Rev. Lett. **80**, 704 (1998).
[33] D. Leppinen and J. R. Lister, Phys. Fluids **15**, 568 (2003).
[34] J. C. Burton, J. E. Rutledge, and P. Taborek, Phys. Rev. Lett. **92**, 244505 (2004).
[35] W. van Hoeve, S. Gekle, J. H. Snoeijer, M. Versluis, M. P. Brenner, and D. Lohse, Phys. Fluids **22**, 122003 (2010).

[36] A. U. Chen, P. K. Notz, and O. A. Basaran, Phys. Rev. Lett. **88**, 174501 (2002).
[37] M. Moseler and U. Landman, Science **289**, 1165 (2000).
[38] J. Eggers, Phys. Rev. Lett. **89**, 084502 (2002).
[39] D. T. Papageorgiou, Phys. Fluids **7**, 1529 (1995).
[40] J. R. Lister and H. A. Stone, Phys. Fluids **10**, 2758 (1998).
[41] I. Cohen, M. P. Brenner, J. Eggers, and S. R. Nagel, Phys. Rev. Lett. **83**, 1147 (1999).
[42] W. W. Zhang and J. R. Lister, Phys. Rev. Lett. **83**, 1151 (1999).
[43] P. Doshi, I. Cohen, W. W. Zhang, M. Siegel, P. Howel, O. A. Basaran, and S. R. Nagel, Science **302**, 1185 (2003).
[44] J. C. Burton, R. Waldrep, and P. Taborek, Phys. Rev. Lett. **94**, 184502 (2005).
[45] S. T. Thoroddsen, T. G. Etoh, and K. Takehara, Phys. Fluids **19**, 042101 (2007).
[46] E. J. Vega, A. J. Acero, J. M. Montanero, M. A. Herrada, and A. M. Gañán-Calvo, Phys. Rev. E **89**, 063012 (2014).
[47] M. R. Khorrami, M. R. Malik, and R. L. Ash, J. Comput. Phys. **81**, 206 (1989).
[48] M. A. Herrada, A. M. Gañán-Calvo, and J. M. Montanero, Phys. Rev. E **88**, 033027 (2013).
[49] M. G. Cabezas, A. Bateni, J. M. Montanero, and A. W. Neumann, Colloids Surf. A **255**, 193 (2005).
[50] E. J. Vega, J. M. Montanero, and C. Ferrera, Measurement **44**, 1300 (2011).
[51] We considered the most intense pulse produced by our shaker while keeping its duration below the capillary time (a typical feature of g-jitter). That pulse caused free-surface oscillations $F - F_0$ of about 20% the static value F_0. Therefore, nonlinear contributions are expected to be significant.
[52] J. M. Montanero, Eur. J. Mech. B: Fluids **22**, 167 (2003).
[53] See Supplemental Material at http://link.aps.org/supplemental/10.1103/PhysRevE.90.013015 for the liquid bridge breakup process.
[54] J. R. Castrejón-Pita, A. A. Castrejón-Pita, E. J. Hinch, J. R. Lister, and I. M. Hutchings, Phys. Rev. E **86**, 015301 (2012).